

# Visualizing patterns of intervertebral disc damage with dual-energy computed tomography: assessment of diagnostic accuracy in an ex vivo spine biophantom

Acta Radiologica  
2022, Vol. 63(8) 1118–1125  
© The Foundation Acta Radiologica  
2021



Article reuse guidelines:  
sagepub.com/journals-permissions  
DOI: 10.1177/02841851211025863  
journals.sagepub.com/home/acr



Julian Pohlan<sup>1</sup> , Carsten Stelbrink<sup>1</sup> , Niklas Tuttle<sup>2</sup>,  
Felix Kubicka<sup>2</sup>, Ho Jung Kwon<sup>1</sup>, Paul Jahnke<sup>1</sup>,  
Friedemann Goehler<sup>1</sup>, Olivia Kershaw<sup>3</sup>, Achim D Gruber<sup>3</sup> ,  
Matthias Pumberger<sup>2</sup> and Torsten Diekhoff<sup>1</sup>

## Abstract

**Background:** Previously, dual-energy computed tomography (DECT) has been established for imaging spinal fractures as an alternative modality to magnetic resonance imaging (MRI).

**Purpose:** To analyze the diagnostic accuracy of DECT in visualizing intervertebral disc (IVD) damage.

**Material and Methods:** The lumbar spine of a Great Dane dog was used as an ex vivo biophantom. DECT was performed as sequential volume technique on a single-source CT scanner. IVDs were imaged before and after an injection of sodium chloride solution and after anterior discectomy in single-source sequential volume DECT technique using 80 and 135 kVp. Chondroitin/Collagen maps (cMaps) were reconstructed at 1 mm and compared with standard CT. Standardized regions of interest (ROI) were placed in the anterior annulus fibrosus, nucleus pulposus, and other sites. Three blinded readers classified all images as intact disc, nucleus lesion, or annulus lesion. Additionally, clinical examples from patients with IVD lesions were retrospectively identified from the radiological database.

**Results:** Interrater reliability was almost perfect with a Fleiss kappa of 0.833 (95% confidence interval [CI] 0.83–0.835) for DECT, compared with 0.780 (95% CI 0.778–0.782) for standard CT. For overall detection accuracy of IVD, DECT achieved 91.0% sensitivity (95% CI 83.6–95.8) and 92.0% specificity (95% CI 80.8–97.8). Standard CT showed 91.0% sensitivity (95% CI 83.6–95.8) and 78.0% specificity (95% CI 64.0–88.5).

**Conclusion:** DECT reliably identified IVD damage in an ex vivo biophantom. Clinical examples of patients with different lesions illustrate the accurate depiction of IVD microstructure. These data emphasize the diagnostic potential of DECT cMaps.

## Keywords

Keywords: Dual-energy computed tomography, intervertebral disc, nucleus pulposus, annulus fibrosus

Date received: 8 February 2021; accepted: 18 May 2021

## Introduction

Presently, patients with microstructural lesions of the intervertebral disc (IVD), require magnetic resonance imaging (MRI) for accurate assessment (1). MRI has high diagnostic accuracy, especially when T2-weighted sequences are combined with T2 mapping and glycosaminoglycan chemical exchange saturation transfer (gagCEST) sequences (2–6). However, unlike computed tomography (CT), MRI is not generally available in

<sup>1</sup>Clinic of Radiology, Charité – Universitätsmedizin Berlin, Humboldt-Universität zu Berlin, Freie Universität Berlin, Berlin, Germany

<sup>2</sup>Department of Spine Surgery, Center for Musculoskeletal Surgery, Charité - Universitätsmedizin Berlin, Humboldt-Universität zu Berlin, Freie Universität Berlin, Berlin, Germany

<sup>3</sup>Department of Veterinary Pathology, Freie Universität Berlin, Berlin, Germany

### Corresponding author:

Julian Pohlan, Charite Universitätsmedizin Berlin, Luisenstrasse 7, Berlin 10117, Germany.

Email: julian.pohlan@charite.de

the emergency setting and remains a time-consuming procedure (7). In addition, some patients with spine pathology cannot undergo MRI because of contraindications, such as cardiac devices, magnetic implants, or claustrophobia (8,9).

CT is often used for detecting infectious sources or for imaging patients with unspecific symptoms (10). However, CT is less useful in diagnosing IVD damage. Dual-energy computed tomography (DECT) provides additional diagnostic information by visualizing collagen-rich soft-tissue structures as in patients with cruciate ligament pathologies (11,12). In addition, meta-data confirm an excellent diagnostic performance of DECT for bone marrow edema (13).

DECT of the IVD is currently being used in imaging spinal fractures (14–16). Virtual non-calcium (VNCa) reconstruction of DECT scans has been shown to allow accurate description of disc morphology in degenerative disc disease (17). Alternatively, cMaps can be generated using three-material decomposition for collagen/chondroitin. These provide a precise depiction of the IVD microstructure (18,19). The diagnostic accuracy of DECT cMaps in different IVD pathologies requires further investigation. In particular, nucleus pulposus (NP) prolapse and discitis are relevant pathologies in the emergency setting or in critical care patients. Potentially, cMaps might also be of use when planning the biopsy route in patients with suspected bacterial discitis.

The aim of the present study was to analyze the diagnostic accuracy of DECT cMaps in identifying different patterns of IVD pathology in an *ex vivo* biophantom. Clinical cases are presented to illustrate the feasibility of visualizing IVD lesions using DECT cMaps.

## Material and Methods

### Phantom

A 3-kg lumbar spine specimen from an adult Great Dane dog was used as a phantom. There were no macroscopic signs of spinal degeneration or pathology, nor was anything known from the documentation. The specimen was cooled for 6 h for transport and brought to room temperature for the experiment. Six intervertebral discs of the lumbar spine were imaged before and after injection of 0.8 mL 0.9% sodium chloride solution per IVD and after anterior discectomy using a surgical blade (Fig. 1). The L3/4 IVD was later excluded because images were degraded by artifacts. Five IVDs in total were included for further analysis. The spine biophantom was surrounded by room air during imaging.

### Imaging

DECT imaging was performed at tube voltages of 80 and 135 kVp on a 320-row single-source CT scanner using sequential volume acquisition (Canon Aquilion Prime; Canon Medical Systems, Otawara, Japan). Two dual-energy volumes were acquired as the phantom exceeded the 16-cm z-axis coverage of the detector. Scans were acquired with ascending tube currents of 60/10, 110/20, 170/30, 230/40, 290/50, 400/70, 510/90, 630/110, 740/130, and 800/150 mA at 80/135 kVp, with an exposure time of 0.5 s.

### Reconstruction

A primary image dataset of 80 and 135 kVp images with a slice thickness of 0.5 mm was generated from the raw data using iterative reconstruction (AIDR-3D standard) and a medium soft-tissue kernel without

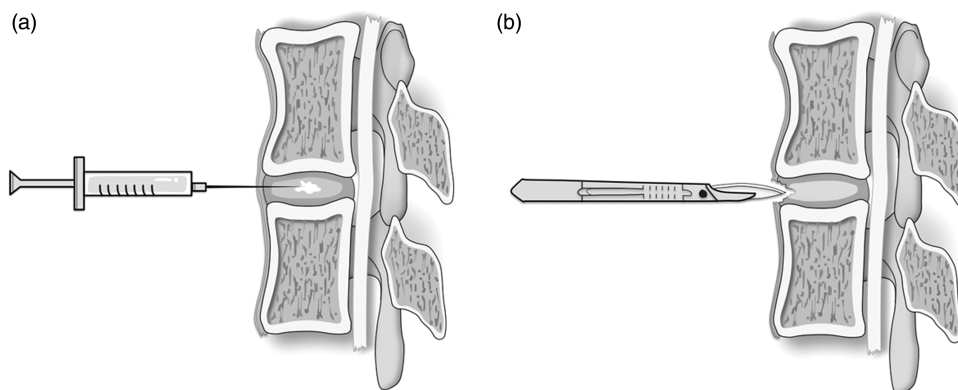


**Fig. 1.** Schematic images showing the preparation of the *ex vivo* spine phantom (a) for inducing the NP lesion by injection of sodium chloride solution and (b) for generating the AAF lesion with a surgical blade. AAF, anterior annulus fibrosus; NP, normal nucleus pulposus.

beam hardening compensation. In a second step, 120 kVp equivalent virtual blended images were reconstructed using an image-data-based weighted average algorithm (Dual-Energy Image View; version 6.0 on the CT-console). cMaps were generated with a raw-data based algorithm (Dual-Energy Raw Data Analysis; version 6.0 on the CT console) using an established gradient of 1.10. Both 120 kVp and cMap image stacks were reconstructed as volumes with a slice thickness of 0.5 mm and reformatted to oblique axial images with a slice thickness of 1 mm for further analysis.

### Reader assessment

For scoring, the images were uploaded into an in-house developed software tool for blinded assessment (20). Three readers scored all 150 images as oblique axial cMaps separately, classifying the appearance as intact disc, nucleus lesion after sodium solution injection, or mechanical annulus lesion. For comparison, the readers scored all 150 images as standard CT in axial reconstruction, separately. A contingency table displays the results of the rating (Table 1). Reader 1 had one year of imaging experience (doctoral candidate), reader 2 had three years of imaging experience (orthopedic surgeon), and reader 3 had five years of imaging experience (radiologist). For scoring, agreement of at least two readers was considered a positive DECT finding.

### Quantitative analysis

Standardized, 15 mm<sup>2</sup> round regions of interest (ROI) were placed in the normal anterior annulus fibrosus (AAF), normal nucleus pulposus (NP), in the NP

lesion, in the AAF lesion, as well as in the paravertebral muscle.

### Analysis and statistics

Student's t-test was performed to compare AAF and NP attenuation values. Signal-to-noise ratio (SNR) and contrast-to-noise ratio (CNR) were calculated. The standard deviation (SD) of paravertebral muscle ROI was used to account for background noise. SNR was calculated by dividing the HU signal of the AAF by the SD of paravertebral muscle. CNR was calculated by subtracting the HU signal of the mechanical lesion of the AAF from the HU signal of the AAF. The resulting value was divided by the SD of the paravertebral muscle.

Correlation analysis was performed for SNR and the number of correct diagnoses using Pearson's test after normality was confirmed for the dataset. Diagnostic accuracy parameters were calculated. Fleiss kappa was calculated for inter-rater reliability. All data were collected in Excel tables for further analysis. Statistical analysis was performed using Prism version 8 (GraphPad, San Diego, CA, USA) and SPSS version 25.0 (IBM Corp., Armonk, NY, USA). A *P* value < 0.05 was considered significant.

### Patient selection

We retrospectively searched the radiology database of our department for patients who underwent DECT of the lumbar spine with different IVD lesions. For the image examples, one patient for each of the following IVD lesions was researched: nucleus lesion;

**Table 1.** Contingency table from a rating with three raters at different levels of experience.\*

	IVD damage +	IVD damage -	Total		IVD damage +	IVD damage -	Total
DECT +	91	4	95	CT +	91	11	102
DECT -	9	46	55	CT -	9	39	48
Total	100	50	150	Total	100	50	150
	NP lesion +	NP lesion -	Total		NP lesion +	NP lesion -	Total
DECT +	41	4	45	CT +	41	11	52
DECT -	9	46	55	CT -	9	39	48
Total	50	50	100	Total	50	50	100
	AAF lesion +	AAF lesion -	Total		AAF lesion +	AAF lesion -	Total
DECT +	50	0	50	CT +	50	0	50
DECT -	0	50	50	CT -	0	50	50
Total	50	50	100	Total	50	50	100

\*DECT cMap assessment is presented as a positive or negative test result against the true lesion as reference standard. IVD damage in general (combining NP and AAF lesions) is compared with NP and AAF lesion separately. Standard CT assessment is provided for comparison. AAF, anterior annulus fibrosus; CI, confidence interval; CT, computed tomography; DECT, dual-energy CT; IVD, intervertebral disc; NP, nucleus pulposus; NPV, negative predictive value; PPV, positive predictive value.

anulus fibrosus lesion; and complete destruction of the IVD.

**Results**

*Phantom*

A total of 150 IVDs were included in the analysis, i.e. IVDs from five different spinal levels measured at 10 different tube currents in three different states: 50 IVDs without pathology; 50 IVDs with NP damage; and

50 IVDs with AAF damage. All discs had a subjectively high density on cMaps compared to bone and surrounding soft tissues, with AAF density being higher than NP density. Images of the ex vivo biophantom are presented in Fig. 2.

*Reader assessment*

The images proved the biophantom to be a suitable model for investigating the identification of different types of IVD pathology of the lumbar spine.

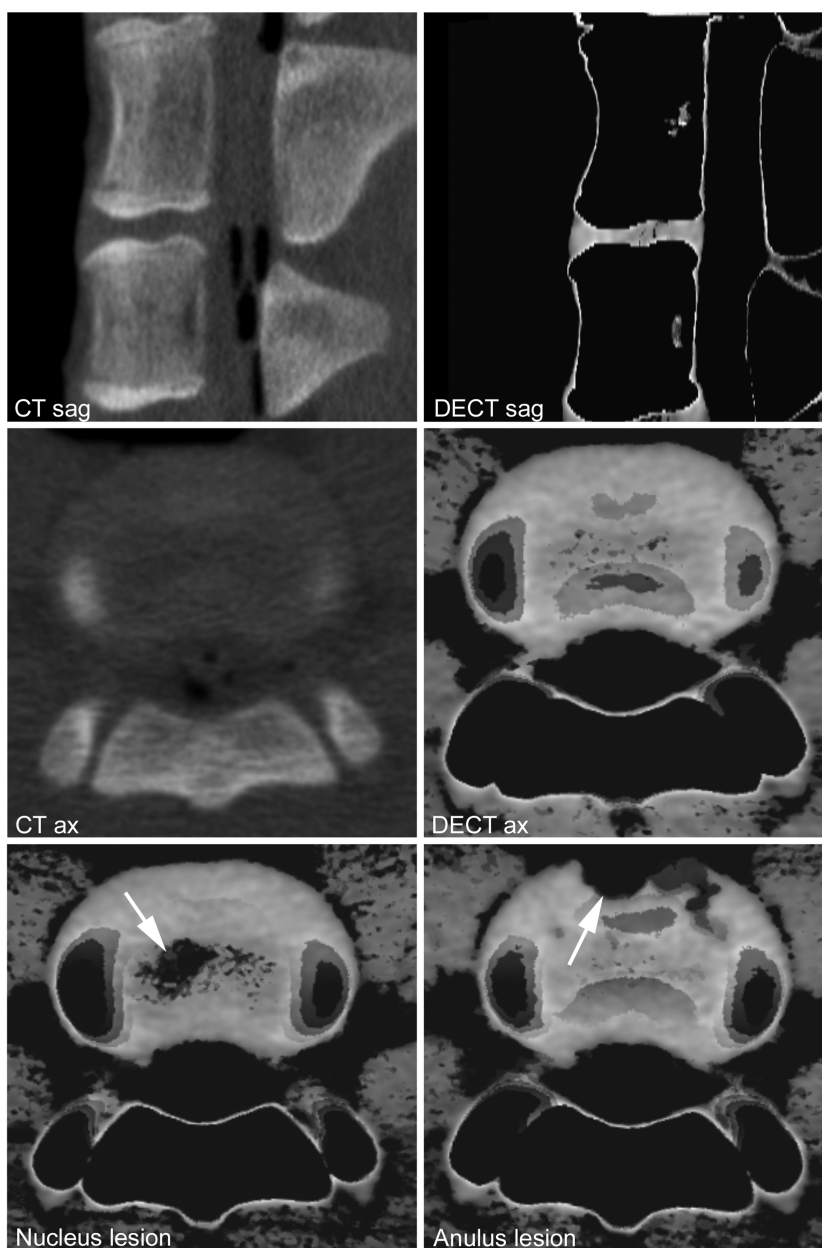


**Fig. 2.** Conventional CT images in sagittal and oblique axial 1-mm reformation. DECT cMaps are shown in axial and sagittal reformation at 1 mm. Different patterns of IVD damage: NP lesion and AAF. AAF, anterior anulus fibrosus; CT, computed tomography; DECT, dual-energy computed tomography; IVD, intervertebral disc; NP, normal nucleus pulposus.

For detection of any IVD damage, DECT cMaps had an overall accuracy of 91.3% (95% confidence interval [CI]=85.6–95.3) with 87.0% (95% CI=78.8–92.9) accuracy for NP lesions and 100% (95% CI=96.4–100) for AAF lesions (Table 2). For comparison, standard CT had an overall accuracy for any IVD damage of 86.7% (95% CI=80.2–91.7). CT accuracy for NP lesions was 80.0% (95% CI=70.8–87.3) and 100.0% (95% CI=96.4–100.0) for AAF lesions.

Analysis of interrater reliability yielded almost perfect agreement with a Fleiss kappa of 0.833 (95% CI=0.831–0.835) for DECT cMaps compared with 0.780 (95% CI=0.778–0.782) for standard CT.

**Table 2.** Accuracy data from a rating with three raters at different levels of experience.\*

	DECT		CT	
	%	95% CI	%	95% CI
<b>IVD damage</b>				
Sensitivity	91.0	83.6–95.8	91.0	83.6–95.8
Specificity	92.0	80.8–97.8	78.0	64.0–88.5
PPV	95.8	89.8–98.3	89.2	83.0–93.3
NPV	83.6	73.2–90.6	81.3	69.6–89.2
<b>NP lesion</b>				
Sensitivity	82.0	68.6–91.4	82.0	68.6–91.4
Specificity	92.0	80.8–97.8	78.0	64.0–88.5
PPV	91.1	79.8–96.4	78.9	68.5–86.5
NPV	83.6	73.8–90.3	70.2	73.8–88.9
<b>AAF lesion</b>				
Sensitivity	100	92.9–100	100	92.9–100
Specificity	100	92.9–100	100	92.9–100
PPV	100	92.9–100	100	92.9–100
NPV	100	92.9–100	100	92.9–100

\*The table shows the sensitivity, specificity as well as positive and negative predictive values for the detection of IVD damage. The data show a moderately higher accuracy of DECT cMaps for NP lesions as compared with standard CT. Both DECT and CT allowed the detection of all AAF lesions.

AAF, anterior anulus fibrosus; CI, confidence interval; CT, computed tomography; DECT, dual-energy CT; IVD, intervertebral disc; NP, nucleus pulposus; NPV, negative predictive value; PPV, positive predictive value.

## SNR/CNR

The mean SNR was  $5.14 \pm 1.97$ . The mean CNR in relation to the AAF signal was  $4.20 \pm 1.81$ . Fig. 3 shows the series of images acquired at ascending tube currents. There was no significant correlation between SNR and the number of correct scoring-based diagnoses made by the readers, though a trend was noted with  $P=0.08$  ( $r=-0.58$ ; 95% CI=-0.89 to 0.07).

## Patients with IVD damage

Three patients with different IVD lesions were identified (Fig. 4). In all three patients, both DECT cMaps and MRI identified the IVD lesion. Patient 1 had an Anderson lesion located centrally in the NP at L3/4 due to axial spondylarthropathy. Patient 2 suffered from degenerative disc disease with a posterior anulus lesion at L3/4 on cMaps. Patient 3 showed complete destruction of the IVD due to bacterial spondylodiscitis at L4/5, with methicillin-sensitive *Staphylococcus aureus* on microbiological testing.

## Discussion

DECT has promising potential for identifying IVD damage based on collagen-/chondroitin-sensitive maps. In our study of an ex vivo biophantom model of a Great Dane dog, we show a high accuracy in the range of 87%–100% for DECT cMaps in the detection of IVD damage. The accuracy of DECT cMaps was slightly higher compared with conventional CT that showed an accuracy of 80%–100%. NP lesions were more difficult to detect than AAF lesions. The lower accuracy for detecting AAF lesions is attributable to the lower inner contrast of IVD structures compared with the strong contrast between air and anterior anulus, where mechanical anulus lesions were located in the phantom. The almost perfect agreement in the analysis of interrater reliability suggests good reliability, even across readers with different levels of experience.

Overall, our results may be of particular interest in the emergency setting, where CT is often more readily

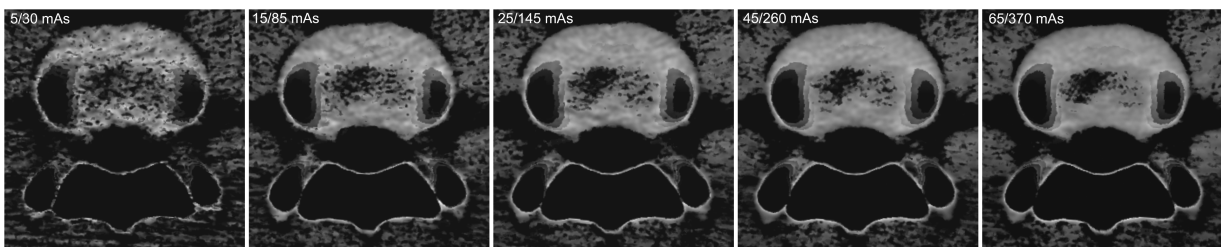


**Fig. 3.** Dose-dependent visualization of a nucleus lesion (cMaps in oblique axial reformation at 1 mm). Images acquired at ascending tube currents from left to right as indicated.



**Fig. 4.** Images obtained in three patients with different spinal pathologies. Images show sagittal and axial reformations at 4 mm including CT, DECT cMaps, and MRI T2 (T1-weighted sagittal MRI scan for patient 1, as no axial image was obtained). Patient 1 has an Anderson lesion located centrally in the nucleus (L3/4). Patient 2 has a posterior anulus lesion at the L4/5 level. Patient 3 shows complete destruction of L4/5 due to bacterial discitis. CT, computed tomography; DECT, dual-energy computed tomography; MRI, magnetic resonance imaging.

available than MRI. Patients with traumatic IVD damage or disc protrusion might benefit from a prompt diagnosis to identify those who require surgery. These data add to existing evidence, which supports using DECT cMaps in IVD imaging. Another field for implementing cMaps might be CT-guided interventions in spondylodiscitis, as DECT might improve biopsy-guidance in partially inflamed tissue. In addition, we supplement our experimental results by providing patient examples of spinal pathologies detected on DECT cMaps including one Anderson lesion in axial spondylarthropathy, one annulus lesion due to degenerative damage, and complete IVD destruction caused by bacterial discitis.

High accuracy in describing IVD morphology and herniation has been reported for conventional CT before (21). DECT has the potential to provide additional information based on the analysis of three-material decomposition. Accordingly, Shinohara et al. (17) used color-coded virtual non-calcium (VNCa) images to detect edematous changes in the IVD and have recently reported highly accurate detection of degenerative IVD changes compared with MRI. Especially in patients with contraindications to MRI such as cardiac devices or claustrophobia, DECT can therefore be a valuable alternative. In the present study, we used a different postprocessing approach to visualize the components of the disc directly. Both collagen and proteoglycans contributed to the density of the IVD on cMaps, which means that DECT cMaps are sensitive to proteoglycans (22).

Recently, we have shown high agreement between DECT cMaps and MRI in the characterization of degenerative disc disease (23). In another study, we demonstrated the diagnostic value of DECT cMaps in the assessment of IVD damage due to osteoporotic vertebral fractures (23).

The present study has some limitations. First, our ex vivo biophantom is a spine from a Great Dane with an IVD size that is different from that of the human IVD. Still, the morphologic similarities suggest that the canine spine is an adequate model of the human spine. Second, the lesions in this experimental setup only partially reflect IVD damage in human spinal pathology. Injection of sodium chloride solution into the IVD does not lead to enzymatic destruction of the connective tissue network as in patients with spondylodiscitis. Moreover, mechanical disruption of the AAF differs from typical human pathologies such as fracture-associated IVD damage in terms of morphology. In addition, the spine model we used in the present study does not include degeneration, which is a common human IVD pathology. Based on our results, however, we conclude that the spine biophantom presented here is a suitable model to mimic different

patterns of IVD damage and evaluate DECT cMaps obtained in an ex vivo setting.

In conclusion, DECT reliably identified IVD damage in an ex vivo biophantom. Clinical examples of patients with different lesions illustrate the accurate depiction of IVD microstructure. These data emphasize the diagnostic potential of DECT cMaps.




#### Declaration of conflicting interests

The author(s) declared no potential conflicts of interest with respect to the research, authorship, and/or publication of this article.

#### Funding

The author(s) received no financial support for the research, authorship, and/or publication of this article.

#### ORCID iDs

Julian Pohlan  <https://orcid.org/0000-0002-5189-4775>  
 Carsten Stelbrink  <https://orcid.org/0000-0001-8970-5610>  
 Achim D Gruber  <https://orcid.org/0000-0002-4502-0393>

#### References

1. Pulickal T, Boos J, Konieczny M, et al. MRI identifies biochemical alterations of intervertebral discs in patients with low back pain and radiculopathy. *Eur Radiol* 2019;29:6443–6446.
2. Haneder S, Apprich SR, Schmitt B, et al. Assessment of glycosaminoglycan content in intervertebral discs using chemical exchange saturation transfer at 3.0 Tesla: preliminary results in patients with low-back pain. *Eur Radiol* 2013;23:861–868.
3. Kim M, Chan Q, Anthony MP, et al. Assessment of glycosaminoglycan distribution in human lumbar intervertebral discs using chemical exchange saturation transfer at 3 T: feasibility and initial experience. *NMR Biomed* 2011;24:1137–1144.
4. Pulickal T, Boos J, Konieczny M, et al. MRI identifies biochemical alterations of intervertebral discs in patients with low back pain and radiculopathy. *Eur Radiol* 2019;29:6443–6446.
5. Xie R, Zhou K, Yuan J, et al. T2 relaxation time for intervertebral disc degeneration in patients with upper back pain: initial results on the clinical use of 3.0 Tesla MRI. *BMC Med Imaging* 2017;17:9.
6. Waldenberg C, Hebelka H, Brisby H, et al. MRI histogram analysis enables objective and continuous classification of intervertebral disc degeneration. *Eur Spine J* 2018;27:1042–1048.
7. Ginde AA, Foianini A, Renner DM, et al. Availability and quality of computed tomography and magnetic resonance imaging equipment in US emergency departments. *Acad Emerg Med* 2008;15:780–783.
8. Russo RJ, Costa HS, Silva PD, et al. Assessing the risks associated with MRI in patients with a pacemaker or defibrillator. *N Engl J Med* 2017;376:755–764.

9. Iwan E, Yang J, Enders J, et al. Patient preferences for development in MRI scanner design: a survey of claustrophobic patients in a randomized study. *Eur Radiol* 2021;31:1325–1335.
10. Pohlan J, Witham D, Muench G, et al. Computed tomography for detection of septic foci: Retrospective analysis of patients presenting to the emergency department. *Clin Imaging* 2021;69:223–227. doi: 10.1016/j.clinimag.2020.09.004. Epub 2020 Sep 19. PMID: 32971451.
11. Jeon JY, Lee SW, Jeong YM, et al. The utility of dual-energy CT collagen material decomposition technique for the visualization of tendon grafts after knee ligament reconstruction. *Eur J Radiol* 2019;116:225–230.
12. Peltola EK, Koskinen SK. Dual-energy computed tomography of cruciate ligament injuries in acute knee trauma. *Skeletal Radiol* 2015;44:1295–1301.
13. Suh CH, Yun SJ, Jin W, et al. Diagnostic performance of dual-energy CT for the detection of bone marrow oedema: a systematic review and meta-analysis. *Eur Radiol* 2018;28:4182–4194.
14. Karaca L, Yuceler Z, Kantarci M, et al. The feasibility of dual-energy CT in differentiation of vertebral compression fractures. *Br J Radiol* 2016;89:20150300.
15. Foti G, Beltramello A, Catania M, et al. Diagnostic accuracy of dual-energy CT and virtual non-calcium techniques to evaluate bone marrow edema in vertebral compression fractures. *Radiol Med* 2019;124:487–494.
16. Jeong SY, Jeon SJ, Seol M, et al. Diagnostic performance of dual-energy computed tomography for detection of acute spinal fractures. *Skeletal Radiol* 2020;49:1589–1595.
17. Shinohara Y, Sasaki F, Ohmura T, et al. Evaluation of lumbar intervertebral disc degeneration using dual energy CT virtual non-calcium imaging. *Eur J Radiol* 2020;124:108817.
18. Pumberger M, Fuchs M, Engelhard N, et al. Disk injury in patients with vertebral fractures—a prospective diagnostic accuracy study using dual-energy computed tomography. *Eur Radiol* 2019;29:4495–4502. doi: 10.1007/s00330-018-5963-4. Epub 2019 Jan 16. PMID: 30649597; PMCID: PMC6610270.
19. Pohlan J, Stelbrink C, Pumberger M, et al. Age-dependent microstructural changes of the intervertebral disc: a validation of proteoglycan-sensitive spectral CT. *Eur Radiol* 2021. doi: 10.1007/s00330-021-08028-z. Epub ahead of print. PMID: 33993329.
20. Conzelmann J, Schwarz FB, Hamm B, Scheel M, Jahnke P. Development of a method to create uniform phantoms for task-based assessment of CT image quality. *J Appl Clin Med Phys* 2020;21:201–208. doi:10.1002/acm2.12974.
21. Notohamiprodjo S, Stahl R, Braunagel M, et al. Diagnostic accuracy of contemporary multidetector computed tomography (MDCT) for the detection of lumbar disc herniation. *Eur Radiol* 2017;27:3443–3451.
22. Pohlan J, Stelbrink C, Pumberger M, et al. Age-dependent microstructural changes of the intervertebral disc: a validation of proteoglycan-sensitive spectral CT. *Eur Radiol*. 2021 May 15. doi: 10.1007/s00330-021-08028-z. Epub ahead of print. PMID: 33993329.
23. Schöinig F, Pumberger M, Palmowski Y, et al. Vertebral disk morphology of the lumbar spine: a retrospective analysis of collagen-sensitive mapping using dual-energy computed tomography. *Skeletal Radiol* 2021;50:1359–1367. doi: 10.1007/s00256-020-03685-5. Epub 2020 Dec 4. PMID: 33277674; PMCID: PMC8119261.